J Mammal Evol
DOI 10.1007/s10914-015-9298-5

ORIGINAL PAPER

First Digital Cranial Endocasts of late Oligocene Notohippidae (Notoungulata): Implications for Endemic South American Ungulates Brain Evolution

María Teresa Dozo[1] · **Gastón Martínez**[1]

Abstract Notohippidae were middle-sized toxodonts recorded from the Eocene to the early Miocene. We provide the first description of the cranial endocasts of *Rhynchippus equinus* and *Eurygenium latirostris* based on three-dimensional reconstructions extracted from high-resolution X-ray computed tomography imagery. The endocasts of *R. equinus* and *E. latirostris* indicate that they were similar in size, proportions of the encephalic components, and neocortical design. The endocranial morphology of these notohippids is very close to that of toxodontids *Adinotherium* and *Nesodon* and differs markedly from both other Toxodontia and Typotheria. Notohippids, together with toxodontids, show the most complex neocortical surface among notoungulates. On the other hand, the neuromorphology of notohippids is in contrast to the neocortical morphological pattern described for Tertiary euungulates (Perissodactyla and Artiodactyla) from the Northern Hemisphere and litoptern Protetotheriidae, South American native euungulates. The relative brain size of *R. equinus* and *E. latirostris* compared with coeval holarctic euungulates from the late Oligocene are significantly below Perissodactyla and near the values obtained for Artiodactyla. Regarding the location of some functional neocortical areas, the expansion of the frontal lobe in Notohippidae may reflect the acquisition of heightened tactile sensitivity in the front of the snout, as recorded in the somatic sensory cortex of living euungulates. The bulging temporal lobe may reflect expansion of the auditory cortex, likely related to the marked enlargement of the middle ear chamber. Both neuromorphological and quantitative data suggest that during the late Paleogene, notohippids developed as complex and encephalized brains as those of the coeval Artiodactyla of northern continents.

Keywords Notoungulata · Notohippidae · Paleoneurology · Cranial endocasts · Computed tomography (CT) · Ungulate brains

Introduction

Notoungulata was the most successful and morphologically diverse group of ungulates during the early and middle Cenozoic of South America (Patterson and Pascual 1972; Reig 1981; Cifelli 1985, 1993; Bond 1986). They underwent a broad radiation that resulted in a variety of forms, including small rodent-like (Interatheriidae), rabbit-like (Hegetotheriidae), medium to large-sized tapir-like, horse-like (Isotemnidae and Notohippidae), and rhino-like (Toxodontidae) forms. However, in spite of this morphological diversity, they constitute a strong clade based on dental and ear features (Cifelli 1993; Billet 2011).

Cifelli's (1993) analysis of notoungulate relationships, and recently, that of Billet (2011) suggest that notoungulates can be divided into two main groups, Toxodontia and Typotheria. The monophyly of these two traditional notoungulates suborders is supported by an original character on the morphology of the ectopterygoid crests.

Notohippidae were middle-sized toxodonts with an early tendency to hypsodonty and considered, to some extent, convergent with the Equidae in regard to some dental features.

Electronic supplementary material The online version of this article (doi:10.1007/s10914-015-9298-5) contains supplementary material, which is available to authorized users.

✉ María Teresa Dozo
dozo@cenpat-conicet.gob.ar

[1] Laboratorio de Paleontología, Centro Nacional Patagónico (CONICET), Boulevard Brown 2915, Puerto Madryn 9120, Chubut, Argentina

Published online: 08 May 2015

Notohippids have been recorded from the Eocene to the early Miocene (López et al. 2010). This group is usually separated into two subfamilies, Rhynchippinae and Notohippinae (Simpson 1945), but the monophyly of the subfamilies, and even the Notohippidae as a clade, has been questioned (Shockey 1997; Marani and Dozo 2005; Cerdeño and Vera 2010; Shockey et al. 2012).

The greatest diversity of Notohippidae has been recorded in the Deseadan localities of La Flecha, Cabeza Blanca, and Scarritt Pocket in Argentine Patagonia (Marani and Dozo 2008) and in the coeval Bolivian locality of Salla (Shockey 1997). Also, several taxa of this age have also been mentioned in Deseadan localities outside Patagonia and Bolivia (Shockey et al. 2009; Cerdeño and Vera 2010) and new material has been recovered from several stratigraphic levels of different ages at Gran Barranca (López et al. 2010).

Three genera of Rhynchippinae are currently recognized for the Deseadan locality of Cabeza Blanca: *Rhynchippus*, *Eurygenium*, and *Morphippus* (Loomis 1914). New findings in this locality, the most complete skulls known for Notohippidae, motivated the start of new studies on *Rhynchippus equinus*, and *Eurygenium latirostris* (Marani and Dozo 2005, 2008). In that regard, the exceptional preservation and application of high resolution X-ray computed tomography allowed the first 3D reconstructions of notohippid skulls and endocasts to be obtained. The increased use of X-ray computed tomography (CT) scan technology has given unprecedented access to the internal structures of fossils, and triggered new interest in mammalian cranial endocast studies (e.g., Conroy and Vannier 1984; Macrini et al. 2006; Sutton 2008; Witmer et al. 2008; Orliac et al. 2012; Orliac and Gilissen 2012).

The study of cranial endocasts is important for at least a couple of reasons. First, the brain is the organ in which sensory information and motor functions are coordinated. Therefore, the evolution of behavior is tied to the evolution of the brain and the study of cranial endocasts of extinct species is a valuable approach for getting clues on their behavior. Second, cranial endocasts represent a potentially large amount of unexplored phylogenetic data (Macrini et al. 2007).

In this work, we provide a detailed description of the first cranial endocasts of *Rhynchippus equinus* and *Eurygenium latirostris* based on three-dimensional reconstructions extracted from computed tomography imagery and compare the virtual endocast of *R. equinus* to the corresponding artificial endocast, too. We also compare notohippid endocasts with those of other notoungulates, living and fossil Euungulata (orders Perissodactyla and Artiodactyla) from the Northern Hemisphere, and with Litopterna Protherotheriidae from South America, which, in some cases, may belong to their ecological equivalent (Table 1, see the electronic Appendix; Simpson 1933a, b; Patterson 1937; Reig 1981). Finally, we infer the location of some functional neocortical areas and analyze the relative brain size with the encephalization quotient (EQ) of Jerison (1973).

Records of Paleoneurological and Endocranial Studies in Notoungulates

Comparative neuroanatomy together with paleoneurology have shown that there is a close cranio-encephalic relationship in most mammals, so that the endocranial casts from modern or extinct animals give a very good image of the external neuroanatomy of the brain (Edinger 1948; Bauchot and

Table 1 Measurements (in mm) of endocranial casts of notoungulates (*CBW* maximum width of cerebellar cast, *CRL* maximum length of cerebral cast exclusive of olfactory bulbs, *CRW* maximum width of cerebral cast, *EL* maximum length of endocast, *FRW* maximum width of frontal region, *OBW* maximum combined width of olfactory bulb casts)

Specimens	EL	CRL	OBW	CRW	CBW	FRW	FRW/CRW ratio	OBW/FRW ratio
Rhynchippus equinus FMNH 13420	99.7	55.5	15	59.6	37.7	36	1: 1.65	1: 2.40
Adinotherium ovinum FMNH 13108	89.7	55.5	18.6	56.2	33.6	37.8	1: 1.48	1: 2.03
Pseudotypotherium sp. FMNH 59292	86.9	44.9	15	48.1	26.2	31.3	1: 1.54	1: 2.09
Interatherium robustum FMNH 13057	41.1	22.9	13.1	23.8	16	15.6	1: 1.52	1: 1.19
Protypotherium sp. FMNH 59289	45.2	25.5	10.4	28.1	17.3	16.6	1: 1.69	1: 1.60
Protypotherium australe FMNH 13002	56.4	29.1	12	32.7	21	17	1: 1.92	1: 1.42
Miocochilius sp. FMNH 59290	68	34.8	14.3	37.7	24.5	18.1	1: 2.08	1: 1.26
Hegetotherium sp. FMNH 13046	51.9	31.8	13.1	35.5	19.2	20.5	1: 1.73	1: 1.56
Hegetotherium mirabile FMNH 59286	57.2	35.3	16.8	39	20.5	19.1	1: 2.04	1: 1.14
Hegetotheriinae indet. CNP-ME 78		33.5		37.8	20.5	18.2	1: 2.08	
Pachyrukhos moyani FMNH 59287		26.7	9	27.3	14.9	12.8	1: 2.13	1: 1.42
Paedotherium chapadmalensis FMNH 59288	39.5	23.4	9.4	29.4	15	14.8	1: 1.98	1: 1.57
Paedotherium sp. CNP-ME 81	39.7	25.6	10.7	29.2	17.4	15.7	1: 1.86	1: 1.47
Paedotherium sp. CNP-ME 82	37.7	23.1	10.8	28.3	13.46	14.3	1: 1.98	1: 1.32

Stephan 1967; Radinsky 1973, 1975, 1981; Dozo 1987, 1994, 1997; Quiroga 1988; Dozo et al. 2004; Macrini 2009). However, the image is not perfect, as noted by the occasional failure of the sylvian fissure in human endocasts to correspond to the real location on the brain or even the marked rhinal fissure in insectivorans that may not correspond to the rhinal fissure on the brain (Jerison 1990). Nevertheless, endocasts provide the best rendering of the brain in the fossil record.

One of the first reports about the endocasts of notoungulates is the paper by Gervais (1872), which presented endocasts of *Toxodon* and *Mesotherium* (ex-"*Typotherium,*" Simpson 1940). Most of the known South American notoungulate endocasts were described by George Gaylord Simpson and Bryan Patterson. Simpson (1932, 1933a, b) described endocasts of Eocene and Miocene notoungulates, and Patterson (1937) described several endocasts of Toxodontidae, Notohippidae, Homalodotheriidae, and Mesotheriidae. Dechaseaux (1958, 1962) reviewed the South American ungulates endocasts and described the first endocast of *Pachyrukhos*, a small Hegetotheriidae. Jerison (1973) analyzed relative brain size in the South American ungulates, and Radinsky (1981) carried out studies on the brain of notoungulates in the context of brain evolution in extinct South American ungulates. Dozo (1997) studied endocasts of the Hegetotheriidae *Paedotherium insigne* and the Caviidae *Dolicavia minuscula* from the Pliocene of Buenos Aires and concluded that the convergence of these mammals, currently established on the basis of dental and postcranial features, is also shown in the neuromorphology. Recently, new studies have provided the first detailed description of the bony labyrinth of the inner ear of a notoungulate, based on a three-dimensional reconstruction extracted from CT imagery of a skull of *Notostylops murinus* (Notostylopidae) (Macrini et al. 2010), the earliest occurrence of ear remains attributed to the Notoungulata from the late Paleocene Beds of Brazil (Billet and de Muizon 2013), and the inner ears of the notoungulates *Altitypotherium chucalensis* (Mesotheriidae), *Pachyrukhos moyani* (Hegetotheriidae), and *Cochilius* sp. (Interatheriidae) (Macrini et al. 2013). These anatomical descriptions of inner ears based on CT scans augment our understanding of this region in notoungulates as a whole, and add to a growing library of anatomical data on the inner ears of mammals in general. Also, these data obtained from CT scan reconstructions can be used to estimate auditory capabilities for the extinct taxa.

Institutional Abbreviations

AMNH, American Museum of Natural History, New York, USA; CNP-ME, endocast collection, Centro Nacional Patagónico, Puerto Madryn, Chubut, Argentina; FMNH, Radinsky collection of the Department of Geology, Field Museum of Natural History, Chicago, USA; IDECH, Instituto de Diagnóstico del Este del Chubut, Argentina; MPEF-PV, Museo Paleontológico Egidio Feruglio, Paleontología Vertebrados, Trelew, Chubut, Argentina; UNPSJB-PV, Repositorio Científico y Didáctico de la Facultad de Ciencias Naturales de la Universidad Nacional de la Patagonia San Juan Bosco, Comodoro Rivadavia, Chubut, Argentina.

Other Abbreviations

SALMA: South American Land Mammal Age

Materials and Methods

Materials

The studied specimens were artificial (CNP-ME 77) and digital endocranial casts taken from the specimen MPEF-PV 695 of the species *Rhynchippus equinus* and a digital endocast from specimen UNPSJB-PV-60 of the species *Eurygenium latirostris*. These specimens are among the most complete skulls known for notohippids (Marani and Dozo 2005, 2008). They are stored in the MPEF-PV and UNPSJB-PV. They were collected in upper levels (Deseadan SALMA, late Oligocene) of the Sarmiento Formation in Cabeza Blanca, southeast of Chubut, Argentina (Loomis 1914; Feruglio 1949; Reguero and Escribano 1996; Sciutto et al. 2000).

For comparative purposes, endocasts of several groups of extinct South American ungulates and extinct North American families of Perissodactyla and Artiodactyla from the endocast collection of Centro Nacional Patagónico (CNP-ME), Radinsky collection of the Department of Geology of the FMNH, and AMNH were added (Table 1, see the electronic Appendix). These data were supplemented with information from the Mammal Brain Collection Internet site of the University of Wisconsin (http://brainmuseum.org) and the literature (Simpson 1932, 1933a, b; Patterson 1937; Brauer and Schober 1970; Radinsky 1978, 1981; Quiroga 1988; Dozo 1997; Macrini 2009).

Methods

Preparation Techniques of Artificial Cranial Endocasts, CT Scanning and Digital Cranial Endocast Extraction

The endocranial cavity of the braincase of *Rhynchippus equinus* (MPEF-PV 695) was prepared mechanically, and an artificial endocast was made constructing a latex internal mould of the endocranial cavity (Radinsky 1968).

The specimens MPEF-PV 695 and UNPSJB-PV-60 were scanned at IDECH, Chubut, Argentina (helicoidal mode)

along the sagittal axis using a voltage of 120 kV (amperage of 30 mA for MPEF-PV 695 and 65 mA for UNPSJB-PV-60). A total of 282 slices were obtained for MPEF-PV 695, pixel size of 0.26 mm, and interslice spacing of 0.8 mm. For UNPSJB-PV-60, a total of 230 slices were obtained, with a pixel size of 0.34 mm and interslice spacing of 0.8 mm. In both cases, the image resolution was 512×512 pixels. The raw scan data were reconstructed using a bone algorithm and exported from the scanner computer in DICOM format.

The data set was cropped to include only anatomical structures of interest (i.e., cranial endocast). Re-slicing of the data along the other two axes, visualization, digital segmentation and 3D reconstructions was performed using 3D Slicer 4.0.1.

Criteria for Neuromorphological Interpretation

Cranial endocasts of both fossil and modern species reflect the external encephalic morphology, and, in extinct mammals, they are the only source of data on the size and shape of brain and the position of neocortical sulci (Radinsky 1978, 1981).

The brain, inferred from the endocast, can be described anatomically with precision. The general development of the neocortex and its regional particularities were studied with respect to the presence or absence of neocortical sulci. In the case of the endocasts, criteria of homology mentioned by Reperant (1971) and discussed by Quiroga (1988) were used to name and interpret the different neocortical sulci: when sulci in the brains of two species are comparable in topographic localization they were treated as homologous. In this work, the Artiodactyla and Perissodactyla (Euungulata, according to Asher and Helgen 2010) have been chosen as reference groups for the identification of neocortical structures in notoungulates. The recent communications by Welker et al. (2015) on proteomics analyses on *Toxodon* reveals that notoungulates may be close allies of Euungulata, particularly Perissodactyla.

The nomenclature used by Kuhlenbeck (1978), Johnson (1990), Welker (1990), and Palombo et al. (2008) to describe the pattern of neocortical sulci in modern euungulates (orders Artiodactyla and Perissodactyla) was followed. The atlas by Brauer and Schober (1970), which describes the brains of many specimens from these orders, was also examined.

The neocortex of euungulates is characterized by the presence of lateral (sulcus lateralis or marginalis), suprasylvian (sulcus suprasylvius), and ectosylvian (sulcus ectosylvius) sulci, with very little development of forebrain flexion (Fig. 1). This results in an elongate brain, with long parallel sulci. In addition to the lateral sulcus, the entolateral (sulcus entolateralis or endomarginalis) and ectolateral (sulcus ectolateralis or ectomarginalis) sulci are observed at its sides. Entolateral, lateral, ectolateral, and suprasylvian sulci divide the neocortex into three convolutions named, in a dorso-lateral direction, marginal or lateral (gyrus lateralis or marginalis),

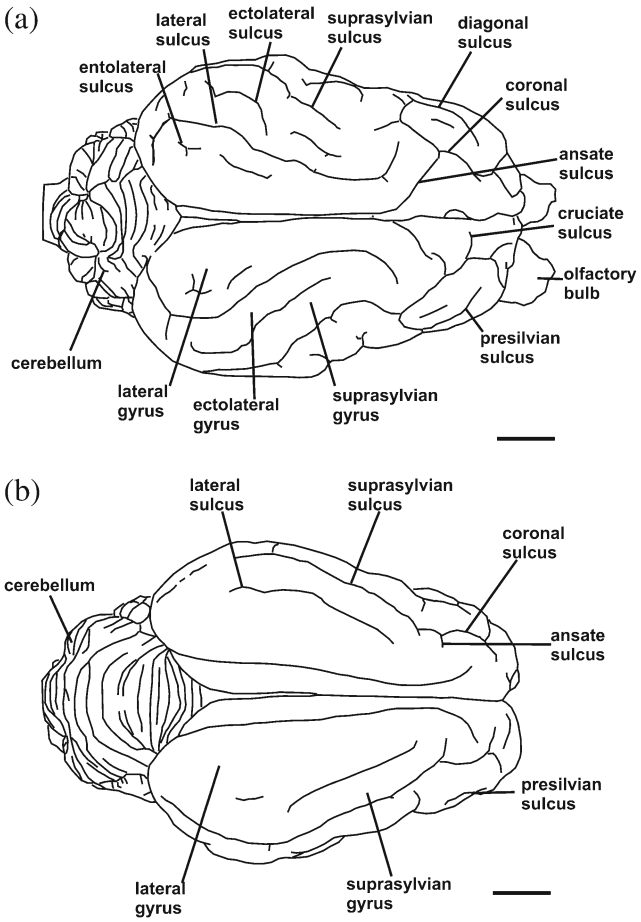

Fig. 1 Pattern of neocortical convolutions in living ungulates. Artiodactyl brains in dorsal view: *Capreolus capreolus* (Cervidae) (**a**), *Moschus moschiferus* (Cervidae) (**b**) (schematic representation summarized of Brauer and Schober 1970). Scale bar=1 cm

ectomarginal or ectolateral (gyrus ectolateralis or ectomarginalis) and suprasylvian (gyrus suprasylvius). The frontal region in living euungulates is well developed with several neocortical sulci. The cruciate sulcus is short, oblique, and running anteriorly and laterally, and the coronal sulcus (sulcus coronalis) continues in the direction of the suprasylvian sulcus or joins the ansate sulcus (sulcus ansatus). Kuhlenbeck (1978) considered the pattern, in general, similar to that of the Carnivora, but the cruciate sulcus, in the frontal region, would have disappeared. However, an alternative interpretation may be that one ascendant extension of the splenial sulcus represents a modified cruciate sulcus, which could have been joined to the splenial system. The coronal and ansate sulci are generally joined as a coronal-ansate sulcus, which can be anastomosed medially with the splenial sulcus and laterally with the lateral sulcus or the suprasylvian sulcus. On the rostral side, between the presylvian and suprasylvian sulci, a diagonal sulcus (sulcus diagonalis) may expand into a ramified system.

Encephalization Quotient

The relative brain size was analyzed with the encephalization quotient (EQ) as defined by Jerison (1973) and Radinsky (1978): EQ1=EV (estimated volume)/0.12 (EM) (estimated body mass)$^{0.67}$, and with the equation defined by Eisenberg (1981): EQ2=EV/0.055 (EM)$^{0.74}$. The latter was based on a regression analysis of empirical data from a large sample of extant placental mammal species, which confirmed the now widely accepted exponent value of about 0.75 for the scaling of brain size to body size among mammals generally (Orliac et al. 2012).

The brain size (EV) was calculated by water displacement of the endocast, including the olfactory bulbs. An estimate of the mass of the brain can be calculated by assuming that brain tissue has a density similar to liquid water (Silcox et al. 2011), which has a specific gravity of 1 g/cm^3. Following Macrini (2009), linear and volumetric measurements were taken on digital endocasts using in this case the measurements module (for linear measurements) and the models module (for volumetric measurements) in 3D Slicer 4.0.1. The same linear measurements were taken on the artificial endocast of MPEF-PV 695 using digital callipers with an accuracy of 0.01 mm to check the reliability of the virtual measurements (Fig. 2; Table 2).

The body mass (BM) was estimated following Mendoza et al. (2006). We applied algorithm 4.1 (log BM=0,736 log SUML+0,606 log SUMW+0,530 log MZW+0,621 log PAW+0,741 log SC – 0,157 log SD+0,603), which estimates body mass from cranial and upper molar measurements (no mandibular measurements are required) (Tables 3 and 4). Although the occipital portion of the skull of specimen UNPSJB-PV-60 is only partially preserved, its cranial architecture and the posterior extent of the endocranial reconstruction allowed us to approximate the length of the posterior portion of the skull (SC). Even assuming that such an approximated value inevitably adds some error to BM estimate, we consider this approach more appropriate than single regression equations, which are generally associated with wide confidence intervals (Mendoza et al. 2006).

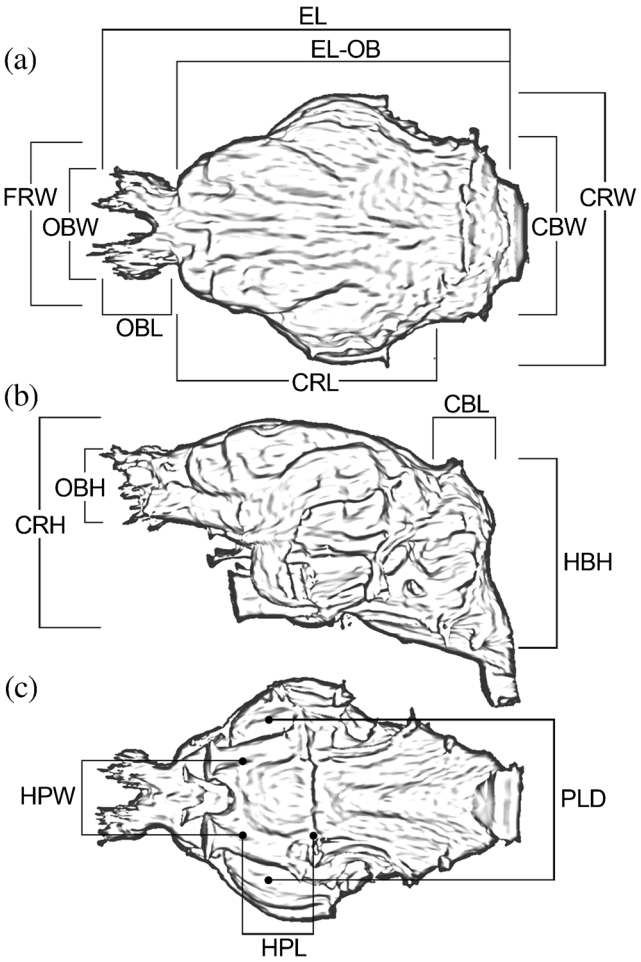

Fig. 2 Line drawing of an endocast of *Rhynchippus equinus* illustrating how measurements were taken (modified from Macrini 2009). (**a**) dorsal view; (**b**) lateral view; (**c**) ventral view. *Abbreviations*: *CBL* maximum length of cerebellar cast, *CBW* maximum width of cerebellar cast, *CRH* maximum height of cerebral cast, *CRL* maximum length of cerebral cast exclusive of olfactory bulbs, *CRW* maximum width of cerebral cast, *EL* maximum length of endocast, *EL-OB* maximum length of endocast exclusive of olfactory bulbs, *FRW* maximum width of frontal region, *HBH* maximum height of hindbrain cast, *HPL* maximum length of hypophysis cast, *HPW* maximum transverse width of hypophysis cast, *OBH* maximum height of olfactory bulb casts, *OBL* maximum length of olfactory bulb casts, *OBW* maximum combined width of olfactory bulb casts, *PLD* maximum distance between ventral edges of piriform lobes

Results

Description of the Cranial Endocasts and Neuromorphological Interpretation

Rhynchippus equinus (MPEF-PV 695) (Figs. 3, 4, 5 and 8)

The artificial (CNP-ME 77) and digital endocranial casts of *Rhynchippus equinus* are described here. These endocasts represent a complete brain showing the cerebral hemispheres, the olfactory bulbs, the ventral surface, and the hindbrain region (cerebellum and brain stem). The maximum width is at the level of the piriform lobes. Measurements of the endocast are provided in Table 2.

Neopallium The neocortical (=isocortical) region is extremely well preserved with well represented neocortical sulci. The telencephalic hemispheres, rhomboid in dorsal view, are well represented and their anterior pole does not cover the olfactory bulbs. Laterally, the telencephalic flexure is pronounced, and a marked antero-posterior sulcus is interpreted as the rhinal fissure. This fissure separates the neocortex (or isocortex) from the ventral paleocortex. It is more distinguishable on its anterior halves and less marked in its middle and posterior region.

Table 2 Measurements for artificial and digital endocasts from *Rhynchippus equinus* (MPEF-PV 695) and digital endocast from *Eurygenium latirostris* (UNPSJB-PV 60). Measurement abbreviations as in Fig. 2

Measurements	Artificial endocast of *R. equinus* (MPEF-PV 695) (mm)	Digital endocast of *R. equinus* (MPEF-PV 695) (mm)	Digital endocast of *E. latirostris* (UNPSJB-PV 60) (mm)
EL	82.86	82.55	–
EL-OB	65.14	64.93	–
CRL	52.05	52.19	52.71
CRW	56.66	58.54	57.03
FRW	34.85	34.70	36.73
CRH	44.14	44.74	43.04[a]
OBL	13.49	15.74	15.80
OBW	18.43	21.10	22.66
OBH	14.68	13.89	15.08
PLD	31.16	31.88	32.23
CBL	12.95	12.56	–
CBW	36.00	37.38	34.16
HBH	39.50	38.47	–
HPL	14.60	14.89	–
HPW	16.49	16.08	–
FRW/CRW ratio	1: 1.62	1: 1.68	1: 1.55
OBW/FRW ratio	1: 1.89	1: 1.64	1: 1.62

[a] Probably lower than the actual value due to the poor preservation of the basicranial and occipital regions

The neocortical region is relatively complex because of a series of neocortical sulci delimiting conspicuous convolutions and a developed sylvian and temporal region. Between the rhinal fissure and the median sulcus, there are impressions of three main sulci. According to their position, they may be treated as equivalent to the ectosylvian, Sylvian or suprasylvian, and lateral sulci. The lateral sulcus lies parallel to the median sulcus. It surrounds the occipital pole of the hemispheres, reaching the frontal region. The Sylvian or suprasylvian sulcus, external to the lateral sulcus, has a shorter antero-posterior course, which is markedly curved when viewed laterally, delimiting a conspicuous temporal lobe. The frontal region is well developed, and a transversal sulcus could be treated as homologous to the ansate sulcus or to the coronal-ansate sulcus. This appears as the fusion of the coronal and ansate sulcus, which is described frequently in the pattern of neocortical sulci in euungulates (Kuhlenbeck 1978). On the rostral side, two depressions could be diagonal and coronal sulci. Between the rhinal fissure and the Sylvian or suprasylvian sulcus, there is another small depression, similar to the ectosylvian sulcus, deeper in its posterior portion. The convolutions are very conspicuous in a dorso-lateral direction and may be treated as homologous to the lateral, suprasylvian, and ectosylvian convolutions. Particularly, the suprasylvian convolution expands anteriorly at the frontal region.

Table 3 Craniodental measurements from *Rhynchippus equinus* (MPEF-PV 695) and *Eurygenium latirostris* (UNPSJB-PV 60. Abbreviations: *MZW* muzzle width, *PAW* palatal width, *SC* length of posterior portion of skull, *SD* depth of face under orbit, *SUMW* second upper molar width, *SUML* second upper molar length. Measurements were taken following Mendoza et al. (2006)

Measurements	*R. equinus* (MPEF-PV 695) (mm)	*E. latirostris* (UNP SJB-PV 60) (mm)
MZW	35.4	56.4
PAW	43.8	59.6
SC	90.0	90.5 *
SD	46.1	46.0
SUMW	16.7	14.0
SUML	21.3	21.3

* Approximated value based on the cranial architecture (see text)

Table 4 Data for relative brain size of *Rhynchippus equinus* (MPEF-PV 695) and *Eurygenium latirostris* (UNPSJB-PV60)

	EBM (Kg)	EV (cm3)	EQ 1	EQ 2
R. equinus	85	**82.143**	0.340	0.335
(MPEF-PV 695)		82.533	0.342	0.337
E. latirostris (UNPSJB-PV60)	119	*77.572	0.256	0.247

EBM estimated body mass using algorithm 4.1 from Mendoza et al. (2006), *EV* endocast volume calculated by water displacement of the endocast (in bold) and by model maker module in 3D Slicer, *EQ1* encephalization quotient using Jerison's equation (1973), *EQ2* encephalization quotient using Eisenberg's equation (1981)

* Probably lower than the actual value due to the poor preservation of the basicranial and occipital regions

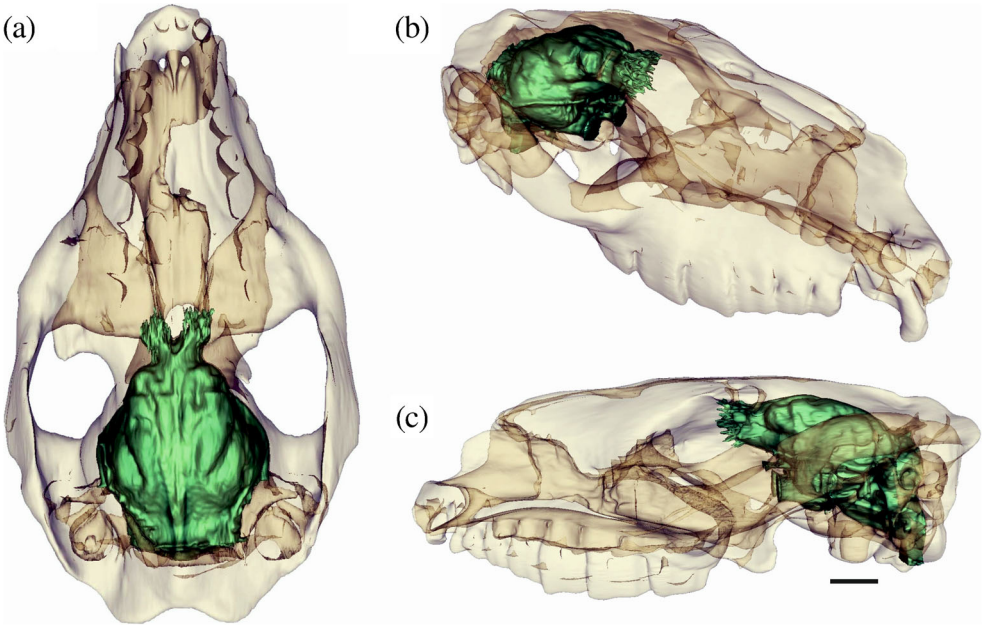

Fig. 3 Skull with bone rendered semi-transparent to reveal the digital cranial endocast of *Rhynchippus equinus* (MPEF-PV 695). Specimen illustrated in dorsal view (**a**), right anterodorsolateral view (**b**), and left lateral (**c**) view. Scale bar=2 cm

Rhinencephalon The paleocortex is represented by the piriform lobe. It is similar in size to the temporo-occipital portion of the neocortex. Rostrally, it is observed as a continuation of the prominent lateral olfactory tract. Ventrally, there are enlarged olfactory tubercles. The casts of the olfactory bulbs are complete and probably reflect their morphology on the brain. They are not covered by the cerebral hemispheres and are connected to the frontal pole by short olfactory peduncles. These bulbs are laterally compressed, small in dorsal view, diverging anteriorly, and narrower than the width of the frontal region. The filling of the foramina of the cribiform plate are visible in front of the olfactory bulbs, indicating endings of the olfactory nerve.

Cerebellum The cerebellum is well represented in the cast. It shows a width smaller than the maximum telencephalic width. The cerebellum is clearly delineated into three parts: a large central vermis and two lateral cerebellar hemispheres. They are separated from the cerebral cast by a transverse fissure, representing the cast of the osseous tentorium cerebelli. The vermis is represented by a somewhat rounded region and separated from the cerebellar hemispheres by two deep paramedian fissures. A small protuberance is seen on the lateral side of cerebellum (cerebellar surface of the petrosal corresponding to the fossa subarcuata) which may represent the paraflocculi (Billet and Muizon 2013).

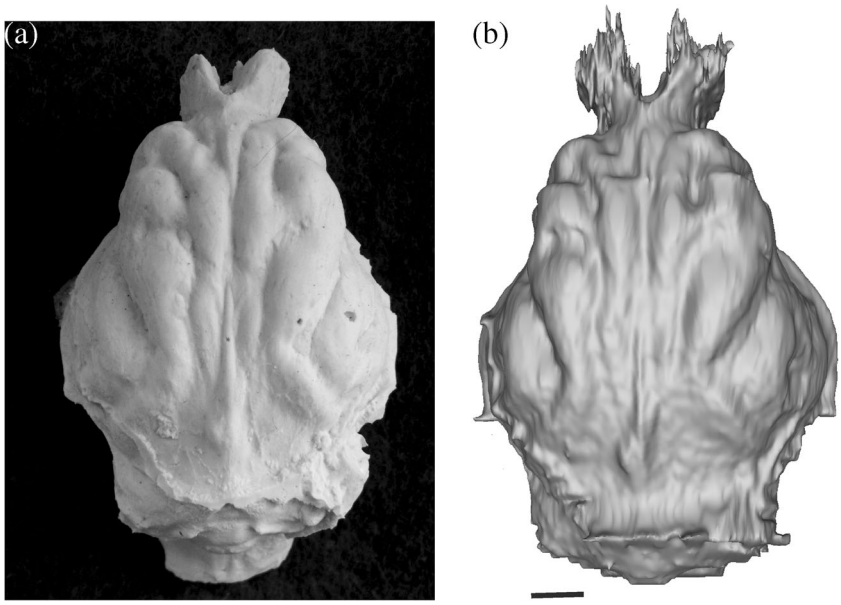

Fig. 4 Artificial (CNP-ME 77) (**a**) and digital (**b**) cranial endocasts of *Rhynchippus equinus* (MPEF-PV 695) from dorsal view. Scale bar=1 cm

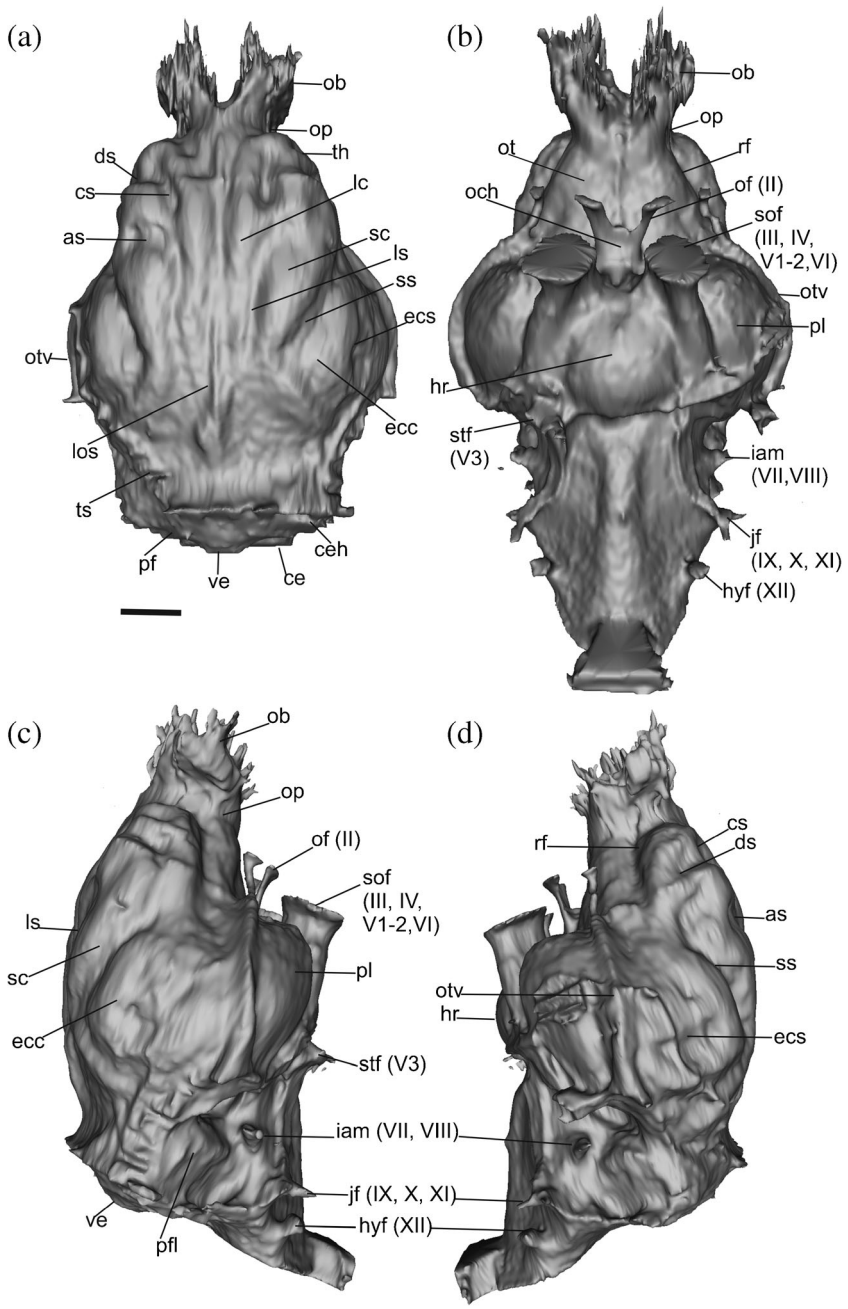

Fig. 5 Digital cranial endocast of *Rhynchippus equinus* (MPEF-PV 695) from dorsal view (**a**), ventral view (**b**), right lateral view (**c**), and left lateral view (**d**). Scale bar=1 cm. *Abbreviations*: *as* ansate sulcus, *ce* cerebellum, *ceh* cerebellar hemisphere, *cs* coronal sulcus, *ds* diagonal sulcus, *ecc* ectosylvian convolution, *ecs* ectosylvian sulcus, *hr* hypophyseal region, *hyf* cast of hypoglossal foramen (exit of cranial nerve XII), *iam* cast of internal auditory meatus (exit of cranial nerves VII, VIII), *jf* cast of jugular foramen (exit of cranial nerves IX, X, XI), *lc* lateral convolution, *los* longitudinal sinus, *ls* lateral sulcus, *ob* olfactory bulbs, *och* optic chiasm, *of* cast of optic foramen (exit of cranial nerve II), *op* olfactory peduncles, *ot* olfactory tubercles, *otv* orbitotemporal vessel, *pf* paramedian fissure, *pfl* paraflocculus, *pl* piriform lobe, *rf* rhinal fissure, *sc* suprasylvian convolution, *sof* cast of sphenorbital fissure (exit of cranial nerves III, IV, V_1 and V_2, VI), *ss* Sylvian or suprasylvian sulcus, *stf* cast of sphenotympanic fissure (exit of cranial nerve V_3), *th* telencephalic hemispheres, *ts* transverse sinus, *ve* vermis

Brainstem, Cranial Nerves and Associated Foramina Several structures are distinguishable on the endocast when viewed ventrally. They are better preserved on the virtual endocast and can be clearly associated with the ventral region of the brain and the exit of cranial nerves. The hypophyseal fossa can be observed on both the virtual and artificial endocasts. The impression of the hypophyseal region is located in the slightly enlarged middle portion and constitutes a large roughly circular deep fossa (Patterson 1937). Rostrally, the impressions of the optic chiasm (chiasma opticum) and optic foramina (exit for the optic nerves, cranial nerve II) are clearly visible. Anterolateral to the hypophyseal fossa is a bulge that likely corresponds to the impression of the sphenorbital fissure. This paired opening transmits the ophthalmic (V_1) and maxillary (V_2) branches of the trigeminal nerve, and the oculomotor (III), trochlear (IV), and abducens (VI) cranial nerves in extant artiodactyls (Macrini 2009) and presumably transmitted the same nerves in notohippids. The cast of the sphenotympanic fissure for the mandibular (V_3) branch of the trigeminal nerve, somewhat deteriorated, seems large (according to Gabbert (2004) there is no oval foramen in toxodontians). Laterally (on both sides of the endocast) and ventromedial to the

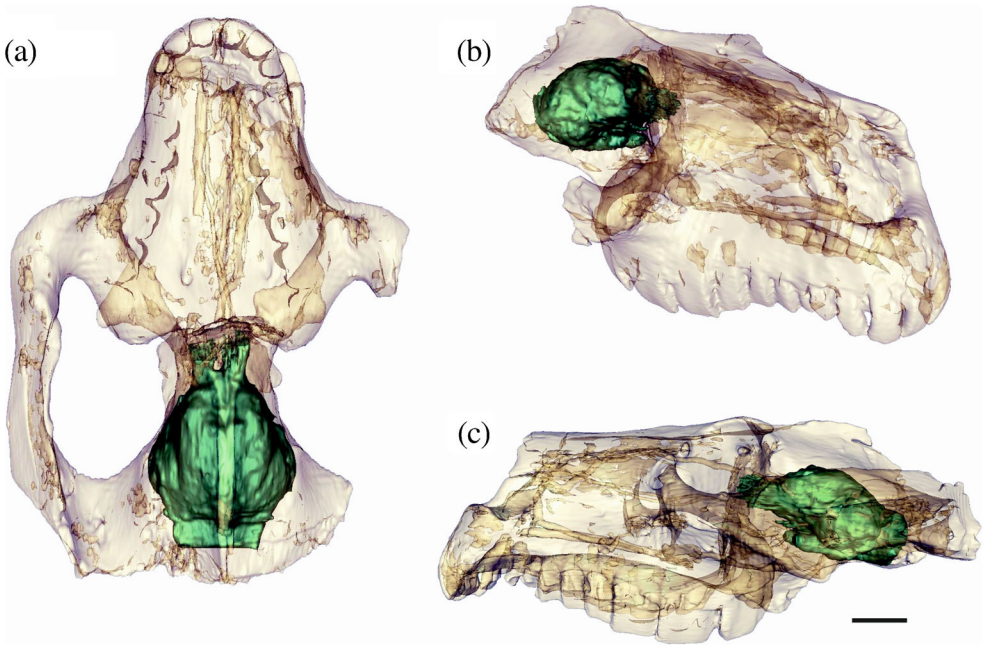

Fig. 6 Skull with bone rendered semi-transparent to reveal the digital cranial endocast of *Eurygenium latirostris* (UNPSJB-PV-60). Specimen illustrated in dorsal view (**a**), right anterodorsolateral view (**b**), and left lateral (**c**) view. Scale bar=2 cm

paraflocculus, notable depressions associated with the petrosal bones are observed. Prominent bumps are clearly distinguishable on the center of these depressions that correspond to the cast of the facial nerve (VII) and of the vestibulocochlear or auditory nerve (VIII), which exit via the internal auditory meatus. The cast of the jugular foramen, which transmits the glossopharyngeal (IX), vagus (X), and spinal accessory (XI) cranial nerves is located posterior and slightly ventral to the cast of the internal auditory meatus (MacPhee 1981: fig. 4). The cast of the hypoglossal foramen (or condylar foramen), which corresponds to the exit of the hypoglossal (XII) cranial nerve, is clearly distinguishable on the side of the medulla oblongata posterior and slightly ventral to the jugular foramen.

Blood Vessels There are two conspicuous venous sinus impressions related to the encephalic and meningeal circulation on the endocast. One is the orbitotemporal vessel (cast of the orbitotemporal groove), as described by Billet and Muizon (2013:466) in notoungulates, which borders medially the lateral side of the piriform lobe. The other is the superior sagittal sinus (or longitudinal sinus), visible at the dorsal midline between the cerebral hemispheres. This sinus is more easily distinguishable on the anterior and posterior portions of the endocast and bifurcates at the caudal end in two transverse structures corresponding to the transverse sinuses.

Eurygenium latirostris UNPSJB-PV-60 (Figs. 6, 7 and 8)

The digital endocast of *E. latirostris* is described here. This endocast represents an incomplete brain showing the cerebral hemispheres, the olfactory bulbs, and the ventral surface. The hindbrain region (cerebellum and brain stem) cannot be reconstructed due to the loss of the back of the skull. The maximum width is at the level of the piriform lobes. Measurements of the endocast are provided in Table 2.

Neopallium The endocranial surface is partially decayed and consequently the neocortical (=isocortical) region and the neocortical sulci cannot be easily distinguished on the digital endocast. As in *R. equinus,* the telencephalic hemispheres, rhomboid in dorsal view, are well represented and their anterior pole does not cover the olfactory bulbs. Laterally, the telencephalic flexure is pronounced, and a weak anteroposterior sulcus is interpreted as the rhinal fissure. Individual convolutions on the surface of the cerebrum cannot be easily distinguished but the neocortical region seems relatively complex with a developed sylvian region. Only the Sylvian or suprasylvian sulcus is observed when viewed laterally, markedly curved, and delimiting a conspicuous temporal lobe. As in *R. equinus*, the frontal region is well developed, but the sulci considered homologous to the ansate sulcus or to the coronal-ansate sulcus cannot be distinguished.

Rhinencephalon The paleocortex is similar to that of *R. equinus*. It is represented by the piriform lobe and as seen in *R. equinus*; it is similar in size to the temporo-occipital portion of the neocortex. As in *R. equinus*, the olfactory bulbs are moderately compressed, and narrower than the width of the frontal region, but arranged in parallel when viewed dorsally.

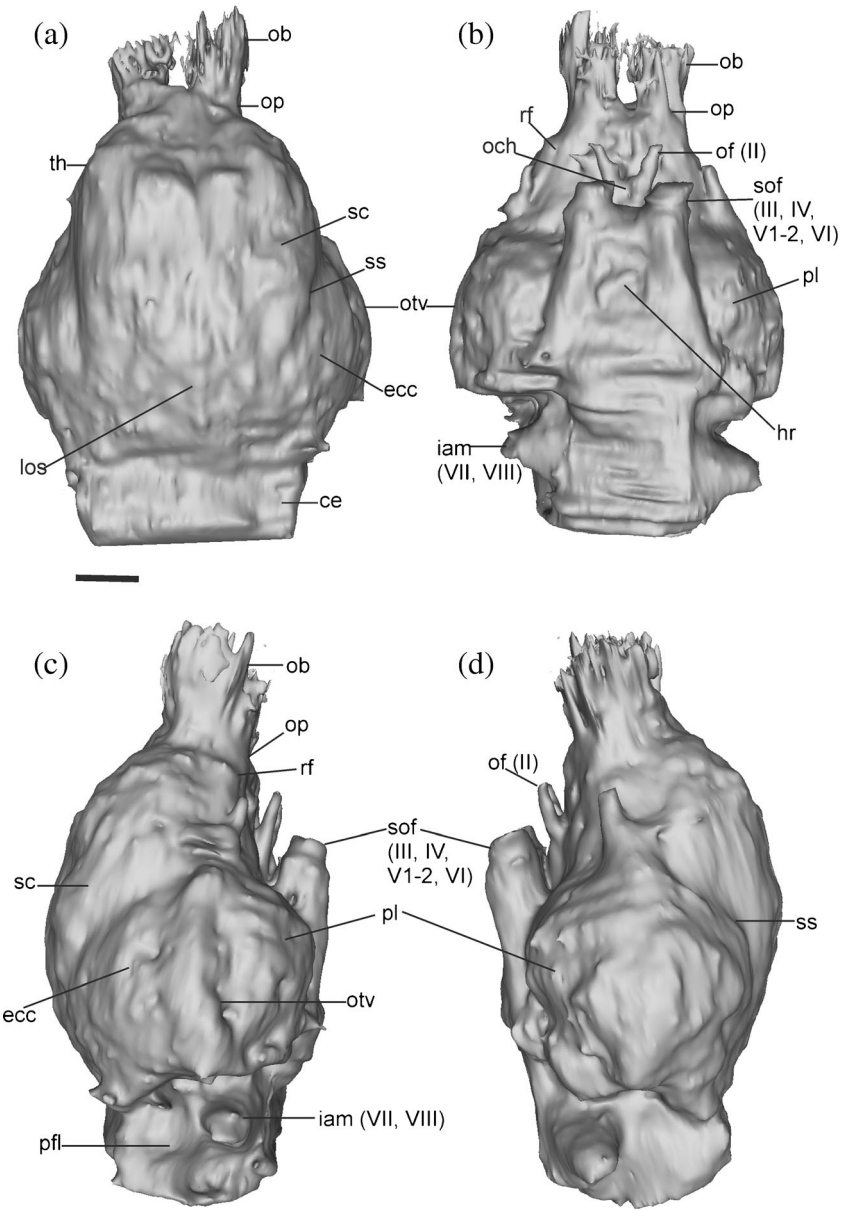

Fig. 7 Digital cranial endocast of *Eurygenium latirostris* (UNPSJB-PV-60) from dorsal view (**a**), ventral view (**b**), right lateral view (**c**), and left lateral view (**d**). Scale bar=1 cm. Abbreviations: as in Fig. 5

Cerebellum Only the proximal portion of the cerebellum is observed. In the dorsal view, it shows a width smaller than the maximum telencephalic width.

Brainstem, Cranial Nerves and Associated Foramina Several structures are distinguishable on the endocast when viewed ventrally, clearly associated with the ventral region of

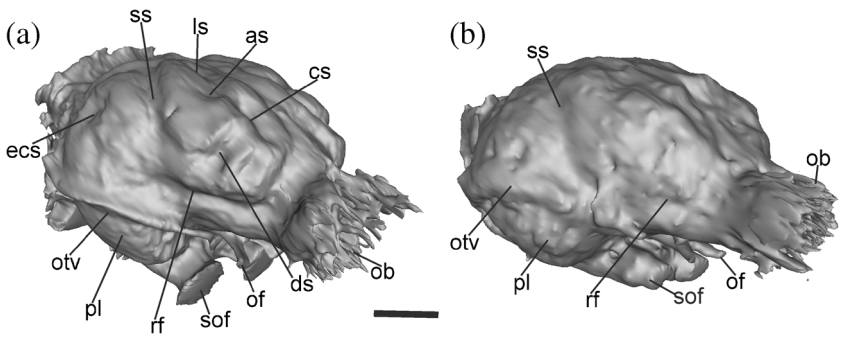

Fig. 8 Comparisons between digital cranial endocasts of *Rhynchippus equinus* (MPEF-PV 695) (**a**) and *Eurygenium latirostris* (UNPSJB-PV-60) (**b**) from right anterodorsolateral view. Scale bar=1 cm. Abbreviations: as in Fig. 5

the brain and the exit of cranial nerves. The impression of the hypophyseal fossa is located in the slightly enlarged middle portion. In front of this zone, there is the impression of the optic chiasm (chiasma opticum) and optic foramina. As in *R. equinus*, anterolateral to the hypophyseal fossa there is a bulge that likely corresponds to the impression of the sphenorbital fissure. Laterally, and ventromedial to the paraflocullus two structures are distinguishable, the cast of the facial nerve and the vestibulocochlear or auditory nerve, which exit via the internal auditory meatus.

Blood Vessels In relation to those structures and impressions of the encephalic and meningeal circulation, because the endocranial surface is partially decayed, there is a weak impression of vessels. Only the orbitotemporal vessel (the imprint of the orbitotemporal groove) that borders the ventral side of the piriform lobe and the superior sagittal sinus (or longitudinal sinus) can be seen.

Relative Brain Size and Encephalization Quotient (EQ)

The endocast volume (EV) of *R. equinus* (MPEF-PV 695) was 82.143 cm^3 (measured by water displacement of the artificial endocast) and 82.533 cm^3 using the model maker module in 3D Slicer. In *E. latirostris* (UNPSJB-PV-60), the EV was 77.572 cm^3 (measured using model maker module in 3D Slicer). However, this value is probably lower than the actual figure due to the poor preservation of the basicranial and occipital regions.

Regarding relative brain size, EQ values were 0.34 for *R. equinus* (calculated with an estimated body mass of 85 Kg) and 0.25 for *E. latirostris* (calculated with an estimated body mass of 119 Kg). Almost the same EQ values were obtained from equation proposed by Jerison (EQ1) and Eisenberg (EQ2) (Table 4).

Discussion

Comparative Neuromorphology with Other Notoungulates

Recent developments in computed tomography and three-dimensional visualization techniques have enabled the non-destructive inspection of the endocast morphology of fossil neurocrania, the basic material for paleoneurological study (Dong 2008; Macrini 2009). Digital endocasts provide a unique source of data for interpreting endocranial anatomy. They afford special information on the shape of the brain that may be lost in conventional anatomical preparations, and provide accurate volumetric and linear measurements of certain gross regions of the brain and its related vascular and nervous structures. Although digital endocasts obtained by 3D reconstruction based on CT scan data are not exact copies of the brain, (because the internal bones show moulds of meninges, sinuses, and cisterns), they conform to the topography of the brain, making it possible to reproduce the external morphology in detail (Macrini 2009).

The digital endocast of *R. equinus* (MPEF-PV 695) shows the rhinal fissure and other cerebral sulci that are also present in an artificial endocast (CNP-ME 77) of the same specimen. However, the digital endocast better reflects the morphology of the olfactory bulbs and exit of the cranial nerves when compared to the artificial endocast. Other anatomical features seen on this endocast, such as casts of arteries and the dorsal sinus system are visible on the digital endocast as well.

Even though obvious differences are observed in cranial morphology, especially regarding the more robust appearance of *E. latirostris*, morphological analysis of the endocasts of *R. equinus* and *E. latirostris* indicates that they were similar in size, in the proportions of the encephalic components (the ratios of width of cerebral cast to width of frontal region and width of olfactory bulb casts to width of frontal region are similar, Table 2), and in neocortical design. Only the olfactory bulbs, which are anteriorly diverging in *R. equinus*, differ from the parallel arrangement observed in *E. latirostris*. In these notohippids, the neocortex (i.e., isocortex), which is more expanded than the ventral paleocortex, has a pronounced telencephalic flexure, a prominent oblique sulcus (the Sylvian or suprasylvian sulcus), and a bulging temporal lobe. In neocorticalized species, the paleocortex always appears laterally reduced, because as the neocortex expands, paleocortical tissue becomes hidden in the rhinal fissure and the piriform lobe and other structures are rotated ventrally (Jerison 1990, 1991; Rowe et al. 2011).

Comparison of these new virtual endocasts with a variety of endocasts from taxa that are closer phylogenetically (Simpson 1933a, b; Patterson 1937; Radinsky 1981; Dozo 1997; see the electronic Appendix) will allow a discussion of the main features regarding their distribution in other notoungulates (Fig. 9). All of this will help to understand brain evolution in notoungulates.

Billet (2011) suggests that notoungulates can be divided into two main groups, Toxodontia and Typotheria. The Toxodontia includes all the large notoungulates and encompasses the families Homalodotheriidae, Leontiniidae, Toxodontidae, and two paraphyletic groups, Isotemnidae and Notohippidae. Two major subclades diverge early within the Typotheria: the Interatheriidae and the clade Archaeohyracidae + Mesotheriidae + Hegetotheriidae. Notostylopids have been considered to be basal among notoungulates (Cifelli 1993) or at least outside the clade uniting Typotheria and Toxodontia.

The endocast of Eocene *Notostylops pendens* (Fig. 9a) shows a triangular cerebrum in dorsal view. The most striking

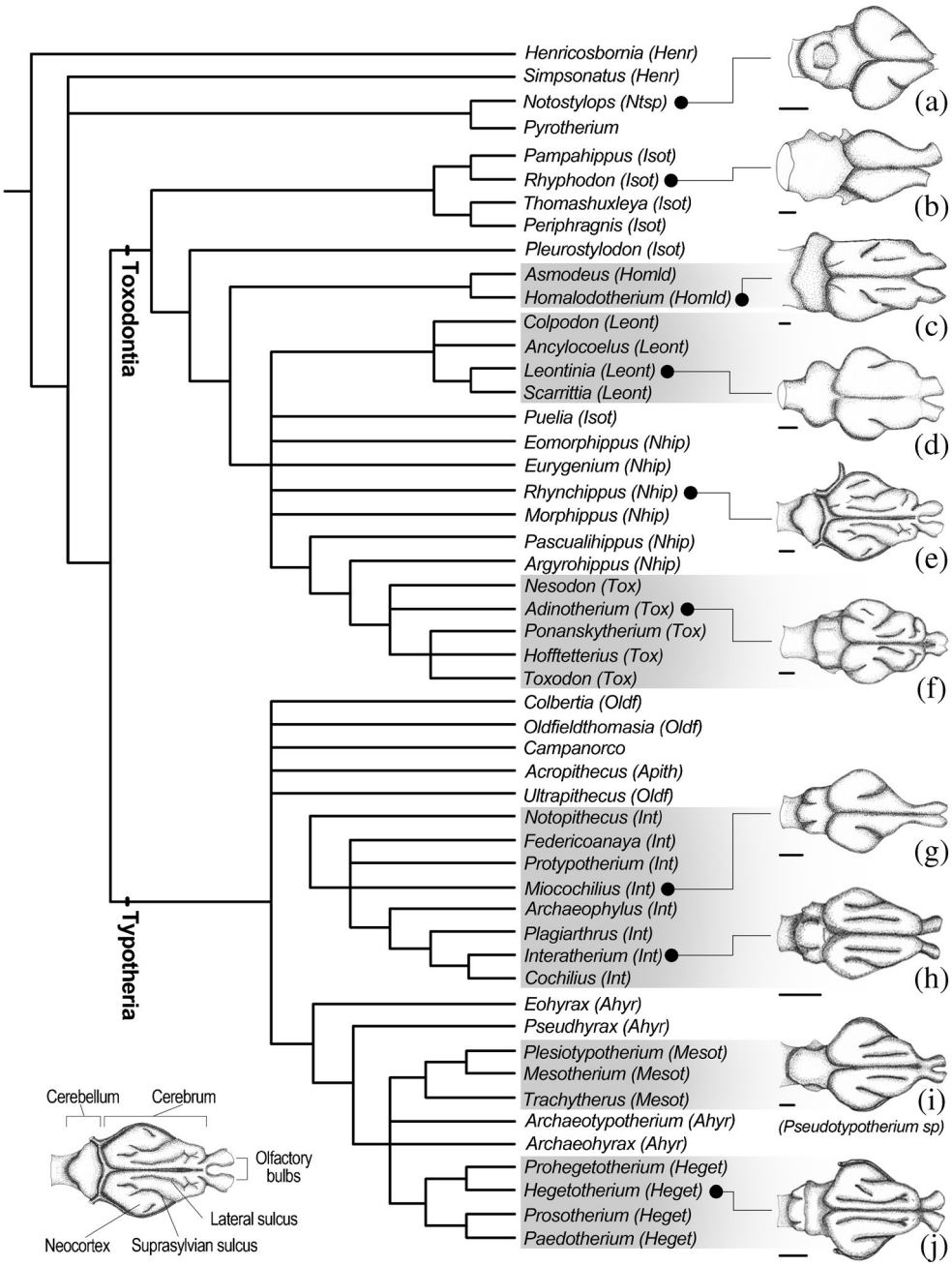

Fig. 9 Phylogenetic relationships of Notoungulata and schematic endocasts of some taxa: (**a**) *Notostylops pendens* (FMNH 59285), (**b**) *Rhyphodon* sp. (FMNH 59282), (**c**) *Homalodotherium* sp. (FMNH 59291), (**d**) *Leontinia* sp. (FMNH 13285), (**e**) *Rhynchippus equinus* (MPEF-PV 695), (**f**) *Adinotherium ovinum* (FMNH 13108), (**g**) *Miocochilius* sp. (FMNH 59290), (**h**) *Interatherium robustum* (FMNH 13057), (**i**) *Pseudotypotherium* sp. (FMNH 59292), and (**j**) *Hegetotherium mirabile* (FMNH 59286). Scale bars=1 cm. *Abbreviations*: *Ahyr* Archaeohyracidae, *Apith* Archaeopithecidae, *Heget* Hegetotheriidae, *Henr* Henricosborniidae, *Homld* Homalodotheriidae, *Int* Interatheriidae, *Isot* Isotemnidae, *Mesot* Mesotheriidae, *Nhip* Notohippidae, *Ntsp* Notostylopidae, *Leont* Leontiniidae, *Oldf* Oldfieldthomasiidae, *Tox* Toxodontidae. Strict consensus cladogram taken and adapted from Billet (2011)

feature of this specimen is the great exposure of the midbrain between cerebrum and cerebellum, a plesiomorphic condition for mammals (Jerison 1990). The neocortex is small with only one neocortical sulcus (Sylvian or suprasylvian sulcus) delimiting narrow frontal lobes from voluminous temporal lobes. The Isotemnidae are the largest Eocene notoungulates but its endocast (*Rhyphodon,* Fig. 9b) shows a neocortex almost smooth and the most unusual feature is that the cerebellum is as wide as the cerebrum. The Homalodotheriidae were large toxodonts. An endocast of a specimen of *Homalodotherium* (Fig. 9c) shows quadrangular telencephalic hemispheres in outline and somewhat wider posteriorly than anteriorly. The neocortex is complex because of the presence of several depressions that are interpreted as neocortical sulci, especially the Sylvian or suprasylvian sulcus. The Leontiniidae are large Oligocene toxodonts. An endocast of a specimen of *Leontinia* (Fig. 9d) displays quadrangular telencephalic hemispheres similar to that of *Homalodotherium* but without neocortical sulci with the exception of the Sylvian or suprasylvian sulcus. The interpreted neuromorphology from the endocasts of notohippids *Rhynchippus* and *Eurygenium* resembles particularly that of toxodontids (Fig. 9e). The same morphology and neocortical design are observed in endocasts of *Adintotherium* (Fig. 9f) and *Nesodon*

(Patterson 1937; Radinsky 1981) from the late early Miocene, except for these toxodontids still have a relatively larger frontal lobe (the ratios of width of cerebral cast to width of frontal region in *Adinotherium* is less than the ratios of *Rhynchippus* and *Eurygenium*, Tables 1 and 2) and an apparently more extensive development of secondary sulci in both the frontal and temporal lobes.

The endocasts of Interatheriidae (Fig. 9h), Mesotheriidae (Fig. 9i), and Hegetotheriidae (Fig. 9j), typotheres that looked like rabbits or large rodents, show similar external brain morphologies including the same pattern of neocortical sulci. The endocasts display the triangular cerebral profile, a bulging temporal lobe, and two main sulci, the Sylvian and lateral sulci. An exception is the interathere *Miocochilius* (Fig. 9g), which shows an endocast with only one neocortical sulcus evident, a prominent Sylvian sulcus, and the olfactory bulbs more pedunculate than in the other typotheres.

Regarding the proportions of encephalic components, Typotheria is different from that of Toxodontia. From the ratios of width of cerebral cast to width of frontal region and width of olfactory bulbs casts to width of frontal region, a larger size for the frontal region is interpreted for Toxodontia than Typotheria (Table 1).

It was not possible to describe a single common encephalic pattern for the order Notoungulata with regard to external brain morphology. However, a pronounced telencephalic flexure, a prominent oblique sulcus (the Sylvian or suprasylvian sulcus), and a bulging temporal lobe are features that characterize the notoungulate neuromorphology (Fig. 9) and were used as diagnostic traits of the order Notoungulata by Madden (1990).

Comparative Neuromorphology with Living and Extinct Euungulata and Litopterna Proterotheriidae

On the other hand, the neuromorphology of notohippids is in contrast to the neocortical morphological pattern described for the brain of living Euungulata (orders Perissodactyla and Artiodactyla) (Kuhlenbeck 1978; Johnson 1990; Welker 1990). As generally observed in the brain of most modern euungulates, the forebrain flexion is not pronounced, favouring the presence of longitudinally arranged sulci that delimitate conspicuous convolutions but without showing a developed Sylvian region. Likewise, this somewhat more simplified pattern is similar to that described by Radinsky (1981) for brains from Tertiary Artiodactyla and Perissodactyla from the Northern Hemisphere and litoptern Proterotheriidae, indigenous ungulates of the South American Tertiary.

The fossil record of North American ungulates brains (Radinsky 1981; Appendix) suggests that during the Oligocene and Miocene, several groups of perissodactyls (e.g., the equid *Mesohippus*) and artiodactyls (e.g., the camelids *Poebrotherium* and *Oxidactylus*) developed brains with similar neuromorphological designs. Neither artiodactyls nor perissodactyls show the Sylvian sulcus and temporal lobe and the neocortex is expanded and folded along longitudinally oriented sulci.

With regard to the Proterotheriidae, the endocasts show good representation of the cerebral hemispheres, rectangular in contour, a well-developed neocortex, and a complex sulcal pattern of longitudinally arranged sulci without forebrain flexure. The first detailed study of an endocast of Proterotheriidae was carried out by Simpson (1933b), who described the plaster endocast of a specimen of "*Proterotherium cavum*" (*Tetramerorhinus lucarius*) of the Santacrucian SALMA (early middle Miocene). Simpson (1933b) described the rhinal fissure and four (lateral, ectolateral, suprasylvian, and ectosylvian) longitudinal neocortical sulci and emphasized that the Sylvian region was not very well developed. Later, Radinsky (1981) and Quiroga (1988) carried out new studies on the brain of the Proterotheriidae. Radinsky (1981) showed the endocasts of three Santacrucian proterotheres ("*Proterotherium,*" *Diadiaphorus,* and *Thoatherium*). He considered there are no oblique Sylvian sulcus and no bulging temporal lobe. Instead, the neocortex is divided by a series of parallel longitudinal sulci that extend for most of the length of the cerebrum. Therefore, endocasts of all three genera are very different from those of the notoungulates. Quiroga (1988) mentioned the endocast of "*Proterotherium cavum*" (*Tetramerorhinus lucarius*), studied by Simpson (1933b), and also described an excellent natural endocast of another specimen of Proterotheriidae from Buenos Aires province without precise origin, but he assigned it to between late Miocene and Pliocene. In that work, he mentioned that the neocortex of both Proterotheriidae showed a clear sulcus pattern of an euungulate mammal (Quiroga 1988:80).

Location of Some Functional Neocortical Areas

The actual locations of the major functional areas of the cortex in extinct specimens cannot be specified, of course, because it is impossible to perform cortical mapping studies in animals that are not alive. However, assuming that the identified neocortical sulci restrict specifiable functional regions, an approximation is possible. Welker et al. (1976) considered the sulci to be reliable indicators of specific functional areas in animal groups that have been studied using neurophysiological and anatomical criteria. In this sense, based on the studies of Welker et al. (1976), Welker (1990), and Johnson (1990) in living ungulates, the location of the somatic sensory cortex, auditory cortex, and visual cortex is interpreted. These cortical regions have been mapped in detail in representatives of artiodactyls (pigs, llamas and sheep) and perissodactyls (horses) (Johnson 1990).

The somatic sensory cortex (SI) lies in the frontal lobe, where three constant sulci occur: the coronal, diagonal, and

anterior suprasylvian sulci. This cortex contains a large tactile projection area that reflects acquisition of heightened tactile sensitivity of lips, rhinarium, and tongue, as expected for a herbivorous lifestyle, but there are no projections from the postcranial body evident in SI (Johnson 1990).

In this regard, the expansion of the frontal lobe in Notohippidae (characteristic feature of Toxodontidae within notoungulates, see ratios in Table 1) may reflect the acquisition of heightened tactile sensitivity in the front of the snout as recorded in the somatic sensory cortex of living euungulates. The general location of the auditory area would be situated in the Sylvian complex (medial to the suprasylvian sulcus, overlapping somatosensory cortex), and the bulging temporal lobe may reflect expansion of this cortex. As mentioned by Radinsky (1981) for the Notoungulata, this feature may be related to the marked enlargement of the middle-ear chambers, which also suggests an auditory specialization. The visual area would be situated dorsal to that, in the region of the lateral gyrus (Johnson 1990; Welker 1990).

Encephalization

The EQ of *E. latirostris* (0.25) is somewhat lower than the EQ of *R. equinus* (0.34). These values clearly differ from that obtained by Radinsky (1981) for the specimen FMNH 13410 of *R. equinus* (EQ=0.93) using the same equation. However, some recent contributions lead us to think that such a difference could be related to BM estimation issues.

Although simple regression equations (as employed by Radinsky) have lower levels of resolution and predictive power than multiple regression methods, the fossil record usually produces fragmentary remains, which precludes researchers to estimate BM from more than just one independent variable (e.g., an osteological measurement). However, almost complete skulls of MPEF-PV 695 and UNPSJB-PV-60 allowed us to estimates BM from different skull measurements following Mendoza et al. (2006). Given the higher potential of multiple regression functions to BM estimation, the difference between our BM estimates and that of Radinsky (1981) is not surprising.

When compared to later BM estimates of Elissamburu (2012), BM estimates provided by Radinsky (1981) are also significantly lower for the majority of genera (*Adinotherium*, *Nesodon*, *Toxodon*, *Protypotherium*, *Typotheriopsis*, *Miocochilius*, *Hegetotherium*, *Homalodotherium*, *Leontinia,* and *Notostylops*). The same can be appreciated when compared to BM estimates obtained by Cassini et al. (2012) for *Astrapotherium magnum*, *Thoatherium minusculum*, *Adinotherium ovinum*, *Adinotherium robustum,* and *Nesodon imbricatus* (among others) based on centroid size.

By contrast, our estimates of 85 kg for *R. equinus* is around BM estimates of 99.67 kg provided by Elissamburu (2012) as the mean value of several estimates obtained from a selection of simple regression equations without considering over- and underestimates. Unfortunately, no previous BM estimates are available for *E. latirostris* in order to compare to BM estimates (119 Kg) obtained in the present contribution. Given this considerations and the aforementioned more accurate performance of multiple regression methods for BM estimation, it seems probable that BM values provided by Radinsky (1981) were underestimated, with a consequent overestimation of EQs. This circumstance prevented us from comparing our data to other toxodonts such as *Adinotherium* and *Nesodon*, whose EQs were also provided by Radinsky (1981).

When compared to similar-sized coeval Holarctic ungulates from the late Oligocene, the EQ of *Rhynchippus* and *Eurygenium* is significantly below Perissodactyla (*Mesohippus*; EQ=0.88) and near the values obtained for Artiodactyla (*Poebrotherium*; EQ=0.36 to 0.42) (Jerison 1973). However, as in the case of Radinsky (1981), comparisons to published data should be carefully considered if BM estimation is based on single anatomical measurements.

Finally, the mean EQs calculated for the extant perissodactyls and artiodactyls (Boddy et al. 2012: table 1) were 1 and 1.42, respectively. This EQ values are significantly larger when compared to extinct euungulates and notoungulates.

Conclusions

The virtual endocasts of notohippids *Rhynchippus equinus* and *Eurygenium latirostris* described herein provide an interesting perspective to understanding notoungulate brain evolution and particularly to improve our understanding of evolution within the Toxodontia.

The endocranial morphology of *R. equinus* and *E. latirostris* are very close to that of the toxodontids *Adinotherium* and *Nesodon* and differs markedly from both other Toxodontia and Typotheria. Notohippids, together with toxodontids, show the most complex neocortical surface among notoungulates, with regard to the development of the temporal lobe, frontal lobe, Sylvian region, presence of the lateral, Sylvian or suprasylvian and ectosylvian sulci, and the development of secondary sulci in both frontal and temporal lobes. These neuroanatomical features are consistent with the derived condition for Notohippidae and Toxodontidae.

On the other hand, the neuromorphology of notohippids is in contrast to the neocortical morphological pattern described for Tertiary euungulates (Perissodactyla and Artiodactyla) from the Northern Hemisphere and litoptern Protetotheriidae, which are indigenous ungulates from South American Tertiary. Neither of these groups show the Sylvian region and temporal lobe, and the neocortex is expanded and folded along longitudinally oriented sulci.

Lastly, both neuromorphological and quantitative data suggest that during the late Paleogene, notohippids developed as complex and encephalized brains as those of the coeval Artiodactyla of northern continents.

Acknowledgments The field work upon which this study was based involved the efforts of many people, including J. Fleagle (Stony Brook University), T. Bown (Erathem-Vanir Geological), R. Taylor (Centro Nacional Patagónico), A. Monti (Universidad Nacional de la Patagonia), R. Vacca (Museo Paleontológico Egidio Feruglio), E. Ruigomez (Museo Paleontológico Egidio Feruglio), and M. Tejedor (Centro Nacional Patagónico). We express our gratitude to A. Venter and family (Estancia El Molino owners) for their hospitality during the field work. We also thank L. Reiner (Museo Paleontológico Egidio Feruglio) for the preparation of the artificial endocast and the CT technologist A. Panes (Instituto de Diagnóstico del Este del Chubut) for guidance and help during the scanning and reconstruction processes. W. Simpson (FMNH) permitted study of the L. Radinsky collection of recent and fossil endocranial casts. Finally, we thank the Editor-in-Chief J. R. Wible and two anonymous reviewers who provided careful reviews that improved the manuscript. This research was conducted under permits from Secretaria de Cultura, Chubut Province, Argentina. It was supported by CONICET PIP 2628 and PICT-SECYT 07/32344.

References

Asher RJ, Helgen KM (2010) Nomenclature and placental mammal phylogeny. BMC Evol Biol 10 (1):102

Bauchot R, Stephan H (1967) Encéphales et moulages endocraniens de quelques insectivores et primates actuels. In: Problemes actuels in paleontologie (Évolution des Vertébrés): Colloques Interanationaux de Centre National de la Recherche Scientifique. Paris, France, 6–11 June 1966. Editions du Centre National de la Recherché Scientifique 163:575–586

Billet G (2011) Phylogeny of the Notoungulata (Mammalia) based on cranial and dental characters. J Syst Palaeontol 9:481–497

Billet G, Muizon C de (2013) External and internal anatomy of a petrosal from the late Paleocene of Itaboraí, Brazil, referred to Notoungulata (Placentalia). J Vertebr Paleontol 33:455–469

Boddy AM, McGowen MR, Sherwood CC, Grossman LI, Goodman M, Wildman DE (2012) Comparative analysis of encephalization in mammals reveals relaxed constraints on anthropoid primate and cetacean brain scaling. J Evol Biol 2:981–994

Bond M (1986) Los ungulados fósiles de Argentina: evolución y paleoambiente. 4° Congreso argentino de Paleontología y Bioestratigrafia (Mendoza) Actas 2:173–185

Brauer K, Schober W (1970) Katalog der Saugetiergehirne. Catalogue of Mammalian Brains. Veb Gustav Fischer Verlag, Jena

Cassini GH, Vizcaíno SF, Bargo MS (2012) Body mass estimation in early Miocene native South American ungulates: a predictive equation based on 3D landmarks. J Zool 287:53–64

Cerdeño E, Vera B (2010) *Mendozahippus fierensis*, gen et sp. nov., new Notohippidae (Notoungulata) from the late Oligocene of Mendoza (Argentina). J Vertebr Paleontol 30:1805–1817

Cifelli R (1985) South American ungulate evolution and extinction. In: Stehli F, Wedd S (eds) The Great American Biotic Interchange. Plenum Press, New York, pp 249–266

Cifelli RL (1993) The phylogeny of the native South American ungulates. In: Szalay FS, Novacek MJ, McKenna MC (eds) Mammal Phylogeny, Volume 2: Placentals. Springer Verlag, New York, pp 195–216

Conroy C, Vannier M (1984) Noninvasive three-dimensional computer imaging of matrix-filled fossil skulls by high-resolution computed tomography. Science 226:456–458

Dechaseaux C (1958) Encéphales de Notongulés. In: Piveteau J (ed) Traité de Paléontologie. Volume VI. Masson et Cie., Paris, pp 121–129

Dechaseaux C (1962) Encéfalos de Notoungulados y de Desdentados Xenartros fósiles. Ameghiniana 2:193–210

Dong W (2008) Virtual cranial endocast of the oldest giant panda (*Ailuropoda microta*) reveals great similarity to that of its extant relative. Naturwissenschaften 95:1079–1083

Dozo MT (1987) The endocranial cast of an early Miocene edentate, *Hapalops indifferens* Ameghino (Mammalia, Edentata, Tardigrada, Megatheriidae). Comparative study with brains of recent sloths. J Hirnforsch 28:397–406

Dozo MT (1994) Interpretación del molde endocraneano de *Eucholoeops fronto*, un Megalonychidae (Mammalia, Xenarthra, Tardigrada) del Mioceno temprano de Patagonia (Argentina). Ameghiniana 31:317–329

Dozo MT (1997) Paleoneurología de *Dolicavia minuscula* (Rodentia, Caviidae) y *Paedotherium insigne* (Notoungulata, Hegetotheriidae) del Plioceno de Buenos Aires, Argentina. Ameghiniana 34:427–435

Dozo MT, Vucetich MG, Candela AM (2004) Skull anatomy and neuromorphology of *Hypsosteiromys axiculus*, a Colhuehuapian Erethizontidae rodent from Chubut, Argentina. J Vertebr Paleontol 24:228–234

Edinger T (1948) Evolution of the horse brain. Geol Soc Am Mem 25:1–177

Eisenberg JF (1981) The Mammalian Radiations: An Analysis of Trends in Evolution, Adaptation and Behavior. University of Chicago Press, Chicago

Elissamburu A (2012) Estimación de la masa corporal en géneros del Orden Notoungulata. Estud Geol (Madr) 68:91–111

Feruglio E (1949) Descripción Geológica de la Patagonia. Buenos Aires: Dirección General de Yacimientos Petrolíferos Fiscales II:1–349

Gabbert SL (2004) The basicranial and posterior cranial anatomy of the families of the Toxodontia. Bull Am Mus Nat Hist 285:177–190

Gervais P (1872) Mémoire sur les formes cérébrales propres à différents groupes de Mammifères. J Zool 1:425–469

Jerison HJ (1973) Evolution of the Brain and Intelligence. Academic Press, New York

Jerison HJ (1990) Fossil evidence on the evolution of the neocortex. In: Jones EG, Peters A (eds) Cerebral Cortex, Vol. 8A. Plenum Press, New York, pp 285–309

Jerison HJ (1991) Fossil, brains and the evolution of the neocortex. In: Finlay BL, Innocenti G, Scheich H (eds) The Neocortex. Ontogeny and Phylogeny. Plenum Press, New York, pp 5–19

Johnson JI (1990) Comparative development of somatic sensory cortex. In: Jones EG, Peters A (eds.) Cerebral Cortex, Vol. 8B. Plenum Press, New York, pp 335–449

Kuhlenbeck H (1978) The Central Nervous System of Vertebrates. Mammalian Telencephalon: Surface Morphology and Central Cortex. The Vertebrate Neuraxis as a Whole. Vol.5, Part II. S. Karger, Basel

Loomis FB (1914) The Deseado Formation of Patagonia. Rumford, Concord

López GM, Ribeiro AM, Bond M (2010) The Notohippidae (Mammalia, Notoungulata) from Gran Barranca: preliminary considerations. In: Madden RH, Carlini AA, Vucetich MG, Kay RF (eds) The Paleontology of Gran Barranca. Cambridge University Press, New York, pp 143–151

MacPhee RDE (1981) Auditory regions of primates and eutherian insectivores: morphology, ontogeny, and character analysis. Contrib Primatol 18:1–282

Macrini TE (2009) Description of a digital cranial endocast of *Bathygenys reevesi* (Merycoidodontidae; Orodontoidea) and implications for apomorphy-based diagnosis of isolated, natural endocasts. J Vertebr Paleontol 29:1199–1211

Macrini TE, Flynn JJ, Croft DA, Wyss AR (2010) Inner ear of a notoungulate placental mammal: anatomical description and examination of potentially phylogenetically informative characters. J Anat 216:600–610

Macrini TE, Flynn JJ, Ni X, Croft DA, Wyss AR (2013) Comparative study of notoungulate (Placentalia, Mammalia) bony labyrinths and new phylogenetically informative inner ear characters. J Anat 223: 442–461

Macrini TE, Rougier GW, Rowe T (2007) Description of a cranial endocast from the fossil mammal *Vincelestes neuquenianus* (Theriiformes) and its relevance to the evolution of endocranial characters in therians. Anat Rec 290:875–892

Macrini TE, Rowe T, Archer M (2006) Description of a cranial endocast from a fossil platypus, *Obdurodon dicksoni* (Monotremata, Ornithorhynchidae), and the relevance of endocranial characters to monotreme monophyly. J Morphol 267:1000–1015

Madden RH (1990) Miocene Toxodontidae (Notoungulata, Mammalia) from Colombia, Ecuador and Chile. Dissertation, Duke University, Durham

Marani H, Dozo MT (2005) Nuevos ejemplares de Rhynchippinae (Notoungulata, Notohippidae) de Edad Deseadense (Oligoceno tardío) del Chubut (Argentina): Sistemática y filogenia. Ameghiniana 42 Suplemento:73R

Marani H, Dozo MT (2008) El cráneo más completo de *Eurygenium latirostris* Ameghino, 1895 (Mammalia, Notoungulata), un Notohippidae del Deseadense (Oligoceno Tardío) de la Patagonia, Argentina. Ameghiniana 45:619–626

Mendoza M, Janis C, Palmqvist P (2006) Estimating the body mass of extinct ungulates: a study on the use of multiple regression. J Zool 270:90–101

Orliac MJ, Argot C, Gilissen E (2012) Digital cranial endocast of *Hyopsodus* (Mammalia, Condylarthra): a case of Paleogene terrestrial echolocation? PLoS ONE 7 e30000:1–10

Orliac MJ, Gilissen E (2012) Virtual endocranial cast of earliest Eocene *Diacodexis* (Artiodactyla, Mammalia) and morphological diversity of early artiodactyls brains. Proc R Soc B 279:3670–3677

Palombo MR, Kohler M, Moya Sola S, Giovinazzo C (2008) Brain versus body mass in endemic ruminant artiodactyls: a case studied of *Myotragus balearicus* and smallest *Candiacervus* species from Mediterranean Islands. Quaternary Internatl 182:160–183

Patterson B (1937) Some notoungulates braincasts. Field Mus Nat Hist Geol Ser 6:273–301

Patterson B, Pascual R (1972) The fossil mammal fauna of South America. In: Keast A, Erk FC, Glass B (eds) Evolution, Mammals, and Southern Continents. State University of New York Press, Albany, pp 247–309

Quiroga JC (1988) Cuantificación de la corteza cerebral en moldes endocraneanos de mamíferos girencéfalos. Procedimiento y aplicación en tres mamíferos extinguidos. Ameghiniana 25:67–84

Radinsky L (1968) A new approach to mammalian cranial analysis, illustrated by examples of prosimian primates. J Morphol 124:167–180

Radinsky L (1973) Evolution of the canid brain. Brain Behav Evol 7: 169–202

Radinsky L (1975) Evolution of the felid brain. Brain Behav Evol 11: 214–254

Radinsky L (1978) Evolution of brain size in carnivores and ungulates. Am Nat 112:815–831

Radinsky L (1981) Brain evolution in extinct South American ungulates. Brain Behav Evol 18:169–187

Reguero MA, Escribano V (1996) *Trachytherus spegazzinianus* Ameghino, 1889 (Notoungulata, Mesotheridae) de la edad Deseadense (Oligoceno superior-Mioceno inferior) de Argentina y Bolivia. Naturalia Patagónica, Ciencias de la Tierra 4:43–71

Reig O (1981) Teoría del origen y desarrollo de la fauna de mamíferos de América del Sur. Museo Municipal de Ciencias Naturales Lorenzo Scaglia, Monografie Naturae 1:1–162

Reperant J (1971) Morphologie compareé de l'encéphale et du moulage endocranien chez les Tylopodes actuels (Mammiferes, Artiodactyles). Bull Mus Natl Hist Nat (3° série) Zool 4:185–321

Rowe TB, Macrini TE, Luo Z-X (2011) Fossil evidence on origin of the mammalian brain. Science 332:955–957

Sciutto JC, Césari O, Escribano V, Pezzuchi H (2000) Hoja Geológica 4566 III Comodoro Rivadavia, Provincia del Chubut. Servicio Minero Argentino, Instituto de Geología y Recursos Minerales. Boletín N° 244

Shockey B (1997) Two new notoungulates (Family Notohippidae) from the Salla beds of Bolivia (Deseadan: late Oligocene): Systematics and functional morphology. J Vertebr Paleontol 17:584–599

Shockey BJ, Flynn JJ, Croft DA, Gans P, Wyss AR (2012) New leontiniid Notoungulata (Mammalia) from Chile and Argentina: comparative anatomy, character analysis, and phylogenetic hypotheses. Am Mus Novitates 3737:1–64

Shockey BJ, Salas Gismondi R, Gans P, Jeong A, Flynn JJ (2009) Paleontology and geochronology of the Deseadan (late Oligocene) of Moquegua, Perú. Am Mus Novitates 3668:1–24

Silcox MT, Dalmyn CK, Hrenchuk A, Bloch JI, Boyer DM, Houde P (2011) Endocranial morphology of *Labidolemur kayi* (Apatemyidae, Apatotheria) and its relevance to the study of brain evolution in Euarchontoglires. J Vertebr Paleontol 31:1314–1325

Simpson GG (1932) Skulls and brains of some mammals from the *Notostylops* beds of Patagonia. Am Mus Novitates 578:1–11

Simpson GG (1933a) Braincasts of *Phenacodus*, *Notostylops* and *Rhyphodon*. Am Mus Novitates 622:1–19

Simpson GG (1933b) Braincasts of two typotheres and a litoptern. Am Mus Novitates 629:1–18

Simpson GG (1940) The names *Mesotherium* and *Typotherium*. Am J Sci 238:518–521

Simpson GG (1945) The principles of classification and a classification of mammals. Bull Am Mus Nat Hist 85:1–350

Sutton MD (2008) Tomographic techniques for the study of exceptionally preserved fossils. Proc R Soc B 275:1587–1593

Welker F, Collins MJ, Thomas JA, Wadsley M, Brace S, Cappellini C, Turvey ST, Reguero M, Gelfo JN, Kramarz A, Burger J, Thomas-Oates J, Ashford DA, Ashton PD, Rowsell K, Porter DM, Kessler B, Fischer R, Baessmann C, Kaspar S, Olsen JV, Kiley P, Elliott JA, Kelstrup CD, Mullin V, Hofreiter M Willerslev E, Hublin J-J, Orlando L, Barnes I, MacPhee RDE (2015) Ancient proteins resolve the evolutionary history of Darwin's South American ungulates. Nature doi:10.1038/nature14249

Welker WI (1990) Why does cerebral cortex fissure and fold? A review of determinants of gyri and sulci. In: Jones EG, Peters A (eds) Cerebral Cortex, Vol. 8B. Plenum Press, New York, pp 3–136

Welker WI, Adrian HO, Lifschitz W, Kaulen R, Caviedes E, Gutman W (1976) Somatic sensory cortex of llama (Lama glama). Brain Behav Evol 13:284–293.

Witmer LM, Ridgely RC, Dufeau DL, Semones MC (2008) Using CT to peer into the past: 3D visualization of the brain and ear regions of birds, crocodiles, and non-avian dinosaurs. In: Endo F, Frey R (eds) Anatomical Imaging: Towards a New Morphology. Springer, New York, pp 67–87